# Metal-like single crystalline boron nanotubes: synthesis and *in situ* study on electric transport and field emission properties†

Fei Liu,[a] Chengmin Shen,[b] Zanjia Su,[a] Xingle Ding,[a] Shaozhi Deng,[a] Jun Chen,[a] Ningsheng Xu*[a] and Hongjun Gao*[b]

*Received 16th September 2009, Accepted 16th December 2009*
*First published as an Advance Article on the web 29th January 2010*
**DOI: 10.1039/b919260c**

Boron nanotubes (BNTs) have been theoretically proposed to have metallic properties whether they are in armchair or zigzag structure, so they have attracted much interest from researchers. However, their real properties have been not understood until now because they are hard to synthesize. In this paper, we have successfully fabricated a large quantity of boron nanotubes, which may provide a way to master their electric and field emission (FE) properties. Study on individual boron nanotubes shows that BNTs have metallic properties with an averaged conductivity of 40 $\Omega^{-1}$cm$^{-1}$. Moreover, individual BNTs can sustain a high current of about 80 μA and their current density can reach $2.04 \times 10^{11}$ A m$^{-2}$, which is very close to those of CNTs. They are also incorporated into prototype luminescent tube devices for the first time and exhibit high luminescent efficiency and stability, which suggests that BNTs have a promising future in the FE area.

## Introduction

Since the report of carbon nanotubes,[1] many efforts have been devoted to the synthesis of nanoscale tubular one-dimensional structures with interest in their future applications, such as nanometre scale electronic, optoelectronic and biochemical-sensing devices.[2–10] Although CNTs have exhibited excellent field emission properties in FE applications, a key problem in preparation process, *i.e.* the control of their chirality, hasn't been solved since they were first found. As know to us, the CNTs can be divided into three types from the point of view of conductivity: metal-like, semiconductor-type and insulator-type, strongly depending on their chirality.[11,12] The large difference existing in their conductivity usually leads to the emission nonuniformity, which limits their further developments in the FE area. So researchers began to look for new kinds of nanomaterials to overcome this technical problem, and boron nanotubes attract most of the interest in the exploring process because of their particular properties. As compared with many non-carbon tubular materials, boron and boron-based structures possess several unique properties: low -density (2.364 g cm$^{-3}$), high melting point over 2300 °C,[13] excellent chemical stability, high thermal conductivity, and high electric conductivity. In addition, metal borides have manifested new properties, such as superconductivity.[14–17] Importantly, recent theoretical studies have shown that, although boron nanotubes (BNTs) have tubular layer structure similar to that of carbon nanotubes (CNTs), they may possess higher electrical conductivity than CNTs.[18–21] Further theoretical calculations indicate that the BNTs possess a metal-like density of states (DOS) and may lead to interesting electrical or optical properties.[16] Unlike CNTs, BNTs may have high conductivity that is chirality-independent. It suggests that all of the BNTs have metal-like properties whether they are in armchair or zigzag structure, which can be beneficial for improving the emission uniformity. So BNTs may be a promising field emission (FE) material if they are synthesized successfully.

Most of the one-dimensional boron nanostructures prepared so far were mainly limited to the form of crystalline or amorphous boron nanowires (BNWs),[22–28] and the reports on BNTs were relatively few.[29] In this paper, we report a successful synthesis of high quality BNTs by a thermal evaporation method. Their crystalline structure and composition were investigated. These BNTs have diameters in a range from 10 to 40 nm and an average length of several micrometres. The mean spacing of adjacent tube layers of the BNTs is about 3.2 Å. Electrical transport and field emission properties of individual boron nanotubes (BNT) and individual boron nanowires (BNW) are compared in detail in order to master the intrinsic properties of boron nanotubes and nanowires. Moreover, the electron affinities of their corresponding nanostructure films are measured by ultraviolet photoelectron spectroscopy (UPS). Both BNTs and BNWs were incorporated into the cathode electrode of an luminescent tube and their FE performance was examined.

---

[a] *State Key Laboratory of Optoelectronic Materials and Technologies, Guangdong Province Key Laboratory of Display Material and Technology, and School of Physics and Engineering, Sun Yat-sen University, Guangzhou, 510275, PR China. E-mail: stsxns@mail.sysu.edu.cn.*

[b] *Beijing National Laboratory for Condensed Matter Physics, Institute of Physics, Chinese Academy of Sciences, Beijing, 100080, PR China. E-mail: hjgao@aphy.iphy.ac.cn*

† Electronic supplementary information (ESI) available: Comparison of the conductivity of BNT with other individual nanostructures; measurements of the luminance stability of Tube I and Tube II in operation; table of the conductivity comparisons of different individual nanostructure; room temperature *I–E* curves of 24 individual BNTs; luminance stability curves of two kinds of luminescent tube in operation. See DOI: 10.1039/b919260c

## Experimental

### Preparation of boron nanotubes

We reported previously the growth of boron nanowires and nanocones synthesized by a thermal evaporation method.[30,31] Later, by varying the experimental conditions, novel morphology of single crystalline BNTs with diameter in a range from 10 to 40 nm was found by thermal reduction of $B_2O_3$ powder. The description of the growth system has been given in our previous papers.[32,33]

In the present study, $Fe_3O_4$ nanoparticles with diameter less than 10 nm were synthesized as catalysts by high temperature solution phase reaction.[34,35] $B_2O_3$ powders (99.99%) mixed with boron powder (99.99%) in a mass ratio of 4 to 3 were ground together as source materials. A two-step increasing temperature procedure was adopted to synthesize the boron nanostructure film: i) when the temperature of the central region of the furnace reached 400 °C, the reaction vessel was maintained in the central region for 20–30 min; ii) the temperature of the reaction region was raised to 1000–1200 °C continually, and the synthesis started. The vessel was kept in the reaction region for 2–4 h and the mean rising rate was 8 °C min$^{-1}$. The flow rate of Ar gas was 300 sccm and the reaction pressure was kept at $1 \times 10^4$ Pa through the experiment. A dark brown or black product was obtained on the surface of the substrate after the furnace was cooled to room temperature.

### Characterization of boron nanotubes

A field-emission type scanning electron microscope (XL-SFEG SEM, FEI Corp.) was used to investigate the morphologies of BNTs. Transmission electron microscopy (Tecnai-20 TEM, PHILIPS) and high-resolution transmission electron microscopy (Tecnai F20 HRTEM, FEI Corp.) were employed to characterize the crystalline structure of BNTs. A Raman spectrometer (Renishaw, inVia) with a charged coupled device (CCD) detector was applied to obtain the Raman spectrum of the boron nanostructure. Measurements of the field emission properties of boron nanostructured film were firstly performed on a UPS (ultraviolet photoelectron spectroscopy) system and a field emission analysis system.

## Results and discussion

By using boron powder (99.99%) and boron oxide powder (99.99%) as source materials and $Fe_3O_4$ nanoparticles as catalyst, we were able to synthesize a large quantity of BNTs on a silicon substrate. After growth for 4 h, a dark film was found on the substrate. Fig. 1A shows the densely-packed boron nanostructures on the silicon substrate, with lengths in the range of 2–4 μm. Fig. 1B is the typical high-resolution SEM (HRSEM) image of the BNTs with the diameters ranging from 10 to 40 nm, in which some boron nanowires are mixed in the product. A side view of a typical BNT is given in Fig. 1C, showing that the free end of the boron nanotube is open. Also, the boron nanotube exhibits a polygonal shape at the open end.

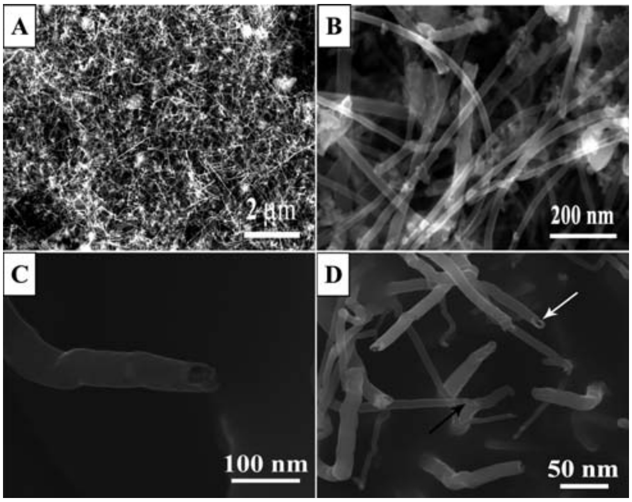

Fig. 1 SEM images of one-dimensional boron nanostructures. (A) Low magnification image of large-area boron nanostructures. (B) The magnified image of the boron nanostructures. (C) The tip of a boron nanotube. (D) High-resolution SEM image of the BNWs and BNTs at the growth stage. Black and white arrows respectively indicate a boron nanotube and a boron nanowire.

To investigate the growth mechanism of BNTs, short BNTs in low density were synthesized with the growth time of 10 min and their high resolution SEM image is shown in Fig. 1D. The white and black arrows respectively indicate the short BNTs and BNWs, which coexisted at the early stage of the growth. It was also found that the catalysts of BNTs or BNWs were just lying on the substrate, indicating that the initial growth precursors of the BNTs should be the alloy nanodroplets of boron-magnetite. This evidence suggests that the growth mechanism of boron nanostructures is the root-growth vapor-liquid-solid (VLS) mechanism. The yield of the BNTs is about 40–50% in the products by calculating their numbers shown in the SEM images.

The morphology of boron nanostructures is sensitive to the experimental conditions, such as the growth temperature and its rising rate, and the ratio of source materials. We also found that the rapid increase of the growth temperature (>30 °C min$^{-1}$) favors the growth of the boron nanowires (BNWs) only. Also, the BNTs can't be grown if the growth temperature is lower than 800 °C. Finally, we found that the ratio of source materials is a key factor for the growth of the BNTs. When the molecular ratio of pure boron powders to $B_2O_3$ powders was adjusted to be lower than 1 : 6, we couldn't find any tubular boron nanostructures in the product.

To better understand the influence factors for the growth of BNTs, we propose the following mechanism. The rising rate of the temperature determines the diffusion rate of boron in the catalyst droplet. The formation of BNTs is directly dependent on the diffusion rate, which can be divided into surface diffusion rate and bulk diffusion rate. Because the shape change of the catalytic particle is strongly related to the wettability of the catalyst and the boron as a function of time, a slower temperature ramp rate will take longer. The size of the catalysts in long growth time at high temperature will be smaller than that in short growth time because the size of the catalyst usually shrinks at high temperature, which suggests that the surface diffusion rate is higher than the bulk diffusion rate.[36,37] When the surface diffusion rate of boron in catalyst droplets is higher than the bulk diffusion rate, boron atoms around the catalyst will firstly reach supersaturation with the process of the reaction and precipitate at the surface of the catalyst, which can't penetrate through the particle. At this root-growth model, the boron clusters only grow along the surface of the catalyst, so the faster rising rate is favorable for the formation of BNTs. Obviously, the ratio of the source materials is also a key factor in preparing BNTs. When the concentration of boron is very high, excessive boron clusters will overburden the catalysts and result in a dominant formation of amorphous boron particles in our observations. Moreover, in this situation the size of the catalyst particles will grow bigger increasing the diffusion difficulty of boron in the catalysts, which leads to the termination of the growth of BNTs.[37,38] For much lower ratio of source materials, the supersaturation of boron in catalyst droplets is hard to occur and the BNTs can't be produced. So only a moderate ratio of source materials is helpful for the formation of BNTs. Many ways have been used to prepare pure BNT films, such as increasing the growth temperature or the rising rate, adjusting the source material ratio or applying new kinds of catalyst. But until now, pure boron nanotubes haven't been fabricated, the endeavor to realize this goal is still in progress.

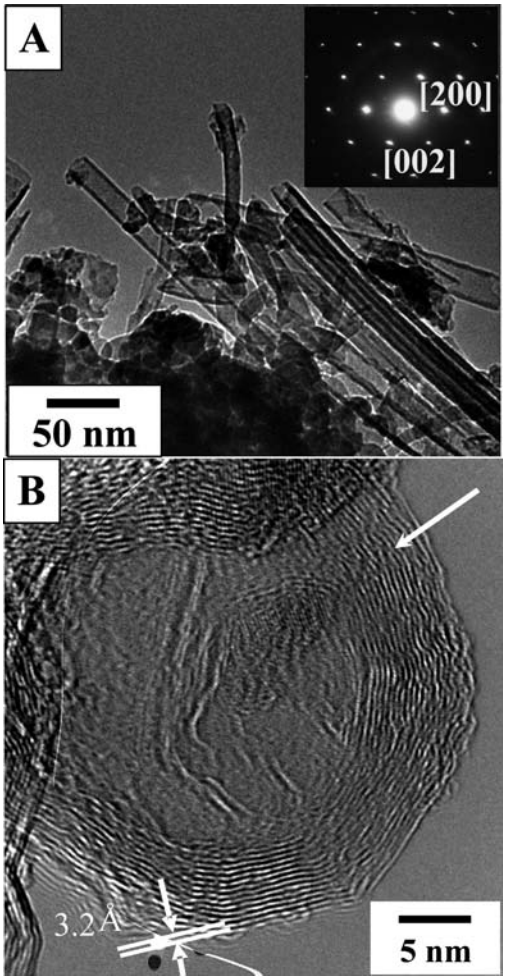

**Fig. 2** TEM and HRTEM images of the boron nanostructures. (A) TEM image of the boron nanostructures of mixed BNWs and BNTs. The inset is the typical SAED pattern of the BNT indicated by the white arrow. (B) The HRTEM images taken from the top of a BNT.

In order to investigate the detailed crystalline structure of the BNTs, TEM and HRTEM were employed. Fig. 2 shows the TEM and HRTEM images of the as-prepared sample. It is seen from Fig. 2A that the product is a mixture of nanotubes and nanowires, which are all straight. The BNTs have lengths of several micrometres and diameters of about 30 nm, and the other nanostructures presented in the TEM image are all boron nanowires. Most of the BNTs have open ends, and their hollow structures are clearly observed from the TEM image. Also, the morphology of BNTs varies, which might correspond to the different geometrical configurations of the boron tubular nanostructure according to the theoretical prediction.[18–21] The selected area electron diffraction (SAED) measurement (inset) shows a sharp spot pattern, suggesting that these nanotubes have good single crystalline structures. The top-view of a typical single BNT is shown in Fig. 2B. The as-synthesized BNTs are multi-layered nanotubes with the spacing between two adjacent layers about 3.2 Å, very close to the theoretical values of 2.997 or 3.021 Å.[18] The layered tubular structure has an inner diameter of about 10 nm and an outer diameter of about 15 nm. The open end of BNTs also exhibits a polygonal morphology. Based on both the SAED pattern and the high-resolution lattice fringes, we conclude that BNTs are perfect single crystals with an α-tetragonal structure. Moreover, BNTs grow along the [001] direction, which is in agreement with the data of the Joint Committee for Powder Diffraction Standards (JCPDS) card No. 73-0511.

We further carried out a study using electron energy loss spectroscopy (EELS) to reveal the elemental compositions of BNTs. From Fig. 3A, strong boron K-edge peaks appear at about 200 eV. Only a small content of oxygen (less than 2%) can be found in the highly magnified EELS spectrum, which may result from the exposure of the sample to the air after the reaction. The small peak at 160 eV can be attributed to the L-edge peak of silicon, coming from the attachment of the silicon substrate during the TEM preparing. Very little content of Cu and C may be found in the higher resolution spectrum, caused by the copper TEM grid covered with carbon film. Gatan EELS analysis shows that the total content of boron through the nanotube is over 96%, thus confirming that as-prepared nanotubes has a thin boron oxide sheath. The tubular structure evident from TEM characterization can also be confirmed by Raman spectroscopy (Fig. 3B). The peak at 210 cm$^{-1}$ (not clearly shown in the figure) is considered as a characteristic peak for tubular structures, corresponding to the radial breathing mode, according to the illustrations in ref. 29. Further, three peaks (b, c and d) appearing between 300 and 600 cm$^{-1}$ can be attributed to different diameters or chirality.[13,29] The other two peaks (e, f) at 625 and 700 cm$^{-1}$ may result from the mixed BNWs with α-tetragonal structure according to ref. 39. Assignment of the other peaks between 900 and 1800 cm$^{-1}$ is in progress.

We also carried out first principles calculation to gain more understanding of as-synthesized BNT structures. We proposed that the quasi-planar and convex structures are the energy favorable boron clusters, which is in agreements with the report results in ref. 20. The most stable layered nanostructures are obtained when the quasiplanar and convex boron clusters are considered as the smallest structural units for the building of BNTs. The density functional theory (DFT) method[40,41] is applied to optimize the geometrical configuration of BNTs. As

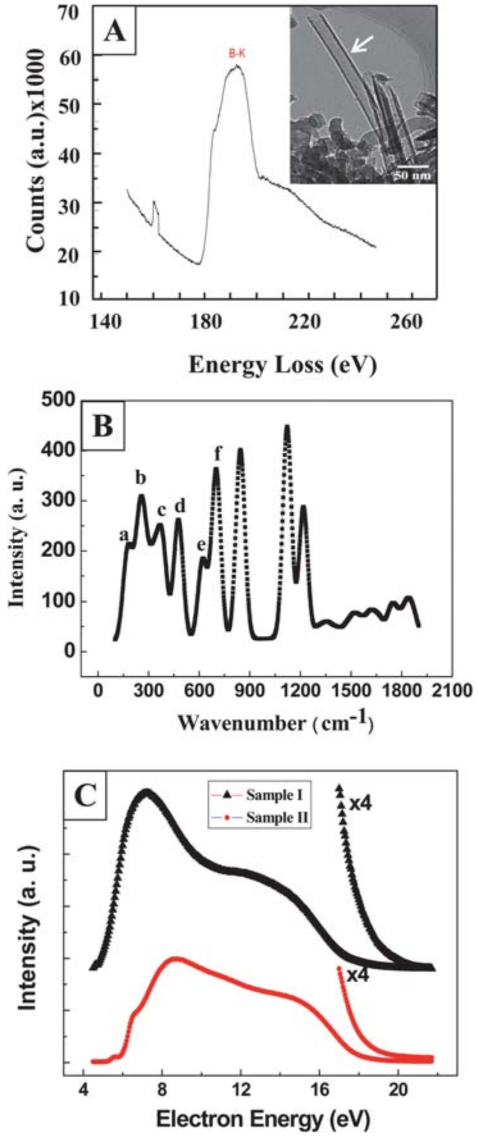

**Fig. 3** (A) The EELS spectrum of an individual BNT. The inset is the TEM image. (B) Typical Raman spectrum of Sample-Type II. (C) The UPS spectra of the as-prepared Sample-Type I and Sample-Type II.

expected, the BNTs by our calculations have faceted surfaces,[42] which conforms to our SEM and HRTEM results in Fig. 1C and 2C. It is worth noting that our current calculation focused on single-walled BNTs. A more complicated model of multi-walled BNTs should offer a more accurate picture of our synthesized structures and this is under investigation.

Boron-based nanostructures have been considered as one of the potential materials for field emission. Their surface electron affinity is one of important factors strongly affecting field emission properties. Ultraviolet photoemission spectroscopy (UPS) is an effective tool to measure the work function or electron affinity (the energy difference between the vacuum level and the bottom of the conduction band) of a semiconductor, which is basing on the energy band diagram of the semiconductor.[43,44] Here we compare the electron affinity of the film containing BNTs and BNWs with that of the pure BNW film on a silicon substrate by using this technique. For simplification, we denoted the pure BNW film as Sample-Type I and the mixed film of BNTs and BNWs as Sample-Type II. These two samples have similar densities and aspect ratios. Fig. 3C shows their corresponding UPS spectra. The low kinetic energy cutoff is magnified by 10 times to obtain more accurate data. The spectral widths ($W_{\text{spectra}}$) of the samples were obtained by linearly extrapolating the emission onset edges to zero intensity at both the low kinetic energy cutoff and the high kinetic end, which are equal to the energy difference between the deep level in the valence band and the edge of the valence band for semiconductor. Based on this method, the widths are determined to be about 15.9 eV and 16.4 eV for Sample-Type I and Sample-Type II, respectively. The surface electron affinity $\chi$ of a sample may be determined using the relation given below:[45]

$$\chi = h\gamma - E_g - W_{\text{spectra}} \tag{1}$$

where $E_g$ is the energy band gap, and $h\gamma = 21.2$ eV, which is the radiation energy of the He I line. The energy band gap of boron nanostructure can be assumed to be the same as that of bulk boron, *i.e.* 1.56 eV.[13,46] Then the $\chi$ values are deduced to be 3.74 eV and 3.24 eV for Sample-Type I and Sample-Type II, respectively. This result may suggest that the BNTs have a lower surface electron affinity than BNWs. Subsequently, we calculate their corresponding surface work function values according to the relation between the work function $\phi$ and the electron affinity $\chi$ in non-doped semiconductors, which is $\phi = \chi + E_g/2$. The obtained work function values are 4.52 eV and 4.02 eV for Sample-Type I and Sample-Type II, respectively, indicating that the work function of BNTs may be lower than that of the bulk boron (about 4.6 eV).[13,46] In addition, as exhibited in Fig. 3C, the overall UPS spectra shapes of Sample-Type I and Sample-Type II are similar, suggesting that Sample-Type II may have an energy band structure resembling that of Sample-Type I. This is possible since the real FE properties of BNT are likely to be smeared out in our UPS measurement due to the mixture of BNWs and BNTs. The real work function of BNT may be concealed by the appearance of the mixture film, and further Kelvin probe force microscopy technology (KPFM) research will be performed on individual boron nanotube in our following work because it is a powerful technique for measuring the work function of materials at the nanoscale.[47,48]

Theoretical studies[18–21] have proposed that BNTs may possess metallic properties which are independent of its tubular structure (*i.e.*, "armchair", "zigzag" or "chiral"), but these were not confirmed experimentally before. Since in our present study a large quantity of BNTs can be fabricated in one sample, we were able to measure the electrical properties of individual BNTs *in situ* using our modified high-vacuum SEM system.[30,49] We carried out the measurements on 15 individual BNTs of Sample-Type II, and typical results of three individual BNTs (A, B and C) were given for comparison in order to understand their intrinsic physical properties. Fig. 4A shows the SEM image of the W probe and the individual BNT ready for measurement, in which the open end of the individual nanotube can be clearly seen. Fig. 4B and C provide the SEM images of the individual boron nanotube and the tungsten probe during the conductivity measurement and during the field emission measurement, respectively. The distance between the individual BNT and

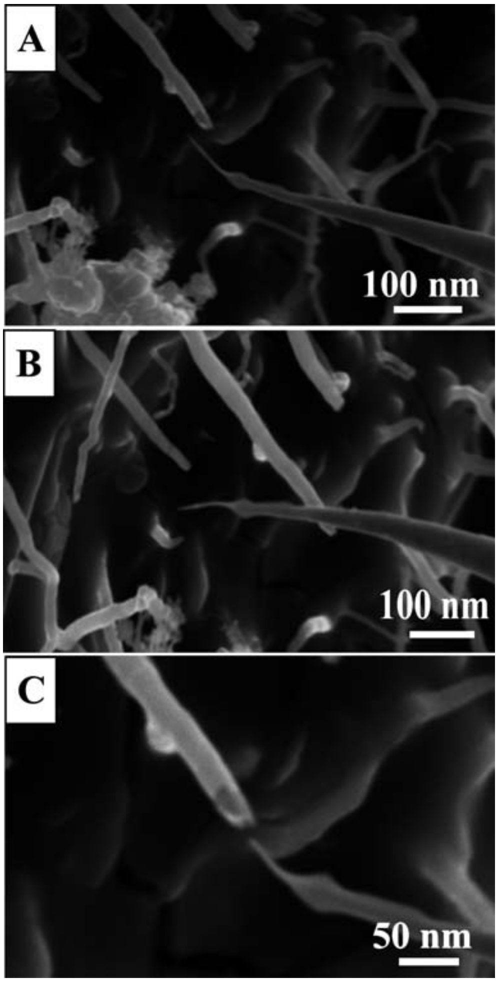

**Fig. 4** The SEM images of the individual BNT and the tungsten probe (A) before the measurement; (B) during the conductivity measurement; (C) during the field emission measurement.

tungsten probe is kept constant at about several micrometres in field emission measurements. Their electric transport properties may be compared by studying the curves in Fig. 5A. The electric transport *I–V* curves of all three individual nanotubes are almost linear, indicating there is a good electrical contact existing between the nanotube and the substrate. Taking the averaged values of outer diameter of 30 nm, inner diameter of 20 nm and length of 3 μm, we determine that Nanotube C has the highest conductivity (36.85 $\Omega^{-1}$cm$^{-1}$) and Nanotube A has the lowest (16.76 $\Omega^{-1}$cm$^{-1}$) among these three nanotubes. These conductivity values of these individual nanotubes are close to the conductivity of a metal (> $10^2$ $\Omega^{-1}$cm$^{-1}$), suggesting that BNTs possess the electrical transport properties comparable to a metal. Also, Table 1 highlights the significant difference in the electric transport properties between individual BNT and individual BNW and the typical conductivity of a BNT is $10^4$–$10^5$ times higher than that of an individual BNW ($\sim10^{-3}$ $\Omega^{-1}$cm$^{-1}$). Finally, we measured 24 individual BNTs and found that their conductivities are in the range of 12–76 $\Omega^{-1}$cm$^{-1}$, which are higher than most of the reported nanostructures and are very close to some reported values of carbon nanotubes ($\sim10^2$ $\Omega^{-1}$cm$^{-1}$).[50–52] Therefore it can be concluded that boron nanotubes have metal-like transport properties. The difference of individual BNTs in the observed conductivity might result from the morphological difference in diameter and length if it is not due to the chirality discrepancy of their tubular structure.

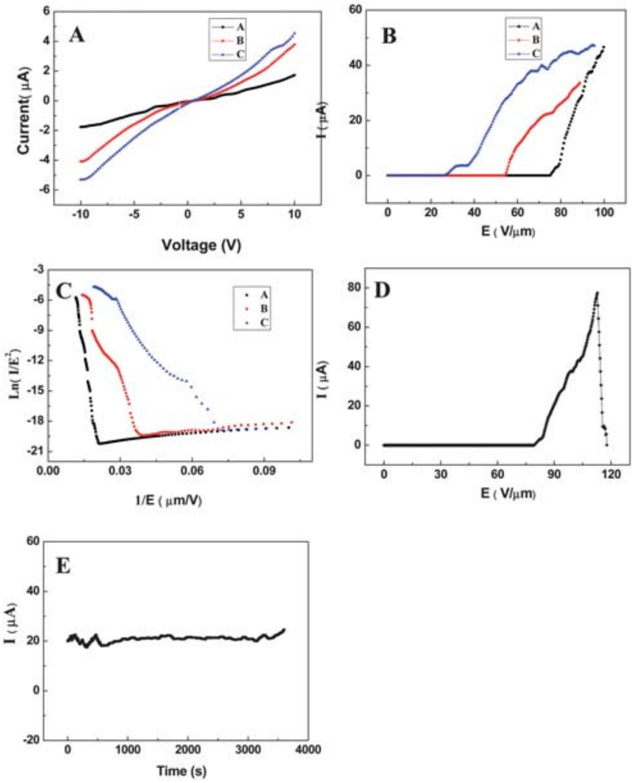

**Fig. 5** (A) The electric transport curves of single BNTs, A, B and C refer to the three different BNTs. (B) The field emission *I–E* curves of the three individual BNTs (A, B and C). (C) Their corresponding FN plots. (D) The typical vacuum breakdown process of a BNT. (E) The typical emission stability curve of a BNT recorded at a high current of 20 μA.

Fig. 5B and C provide the plots of field emission current *versus* electrical field (*I–E*) and their corresponding Fowler-Nordheim (FN) plots. The distance between the individual BNT and the tungsten probe is kept at a constant of about several micrometres in field emission measurements. The individual BNTs have an averaged 1 nA field of about 50 V μm$^{-1}$ (1 nA field is defined as the field required to obtain a total current of 1 nA) and 1 μA field of 55 V μm$^{-1}$ (1 μA field is defined as the field required to obtain a total current of 1 μA), and they are much lower than those of typical individual BNWs (90 V μm$^{-1}$ and 110 V μm$^{-1}$). Nanotube C has the best field emission performance and Nanotube A has the worst among these three nanotubes. By summarizing the electric transport and FE properties of the three BNTs (Table 1), one can see that the nanotube with the highest conductivity has the best field emission performance.[53]

In Fig. 5C, it is obvious that the FN plots of all individual BNTs can be divided into two segments. As for different behaviors of the FN plots of individual nanotubes at low currents and high currents, we believe that the existence of thermal-emission current at high field enhances the field-emission current, and thus results in the nonlinearity, which resembles the illustration on an individual nanowire.[30] In our previous paper, we have reported that a carbon nanotube at high emission

**Table 1** List of the electric transport and FE properties of individual BNTs and BNWs

| Individual nanostructure | | Conductivity/ $\Omega^{-1}$ cm$^{-1}$ | 1 nA field/V μm$^{-1}$ | 1 μA field/V μm$^{-1}$ | Maximum current/μA | $\beta$ (low field) | Breakdown field/V μm$^{-1}$ | Emission Instability |
|---|---|---|---|---|---|---|---|---|
| nanotube | A | 16.76 | 74.8 | 75.8 | 34 | 3596 | 112.8 | 23% (at 20 μA) |
| | B | 24.84 | 54.2 | 54.6 | 47.7 | 8766 | | |
| | C | 36.85 | 26.1 | 28.2 | 88.9 | 19130 | | |
| nanowire (average value) | | $5 \times 10^{-3}$ | 90 | 110 | 2 | 3000 | 225 | 30% (at 10 μA) |

current will reach high temperature in experiments and the emission current is composed of the field emission current and the thermal emission current.[54] This is in agreement with the research results of other groups that the emission current consists of two kinds of emission current and the thermal emission current will be dominant at high current, which leads to the increase of the FN plots.[55,58] The enhancement factor $\beta$ of these individual BNTs is calculated to be about 7000–10000 at low electric fields and 1000–3000 at high electric fields, which is higher than those of individual BNWs. The higher enhancement factor value of individual BNT suggests that it has much higher amplification of electric field than nanowire base on the FN theory, and thus it should exhibit more excellent behavior, which is in good agreement with our recorded emission data in Table 1. In addition, the wide range of $\beta$ values of individual nanotubes implies that they can be widely used for various FE applications.

Furthermore, the emission stability of individual BNT and its endurance ability at high working current were investigated, which are vital factors in determining the FE performance of a working emitter. The typical BNT vacuum breakdown process is shown in Fig. 5D, revealing that individual BNTs can work fine until the emission current reaches about 80 μA. The cross-section area $A$ of a BNT may be obtained using the following expression:

$$A = \pi(r_{\mathrm{out}}^2 - r_{\mathrm{in}}^2) \qquad (2)$$

where $r_{\mathrm{out}}$ and $r_{\mathrm{in}}$ are respectively the averaged outer (30 nm) and inner diameter (20 nm) of the BNT. A typical value of $A$ is about $3.925 \times 10^{-16}$ m$^2$. Thus the upper limit of emission current density can reach $2.04 \times 10^{11}$ A m$^{-2}$, which is comparable to that of the CNTs reported so far ($10^{11}$–$10^{12}$ A m$^{-2}$),[51,56,57] suggesting that BNTs have good endurance to high working current density. In addition, with reference to Table 1, the maximum emission currents (~40–80 μA) of an individual nanotube are about 20–40 times higher than that (~2 μA) of a typical individual nanowire. The vacuum breakdown field (112.8 V μm$^{-1}$) of an individual nanotube is almost half of that of an individual nanowire (225 V μm$^{-1}$). This may be understood since the cathode vacuum breakdown is dependent on Joule heating, rather than applied gap field.[58,59] For an individual BNT, it can reach much higher current than an individual BNW. In addition, the emission current endurance of individual BNTs is found to be two times higher than that of the CNTs in the reports (8–20 μA),[56,60,61] which suggests that BNTs are better than CNTs in the application of high-power microwave tubes and high-current point sources. We do not know at this stage if the melting point of an individual nanotube is different that of an individual nanowire, and if it affects their vacuum breakdown behaviour.

Typical FE stability over time of an individual nanotube at high working current is shown in Fig. 5E. The direct current (DC) field was fixed at 90 V μm$^{-1}$ and the emission current was 20 μA at the beginning. The whole measurement lasted for 1 h. The fluctuation is less than 22%, which is better than that of an individual nanowire (30% at 1 μA). Meanwhile, the 22% instability at high current of 20 μA is acceptable for these reasons: 1) part of the current fluctuation results from the vibrations of vacuum pumps that leads to a slightly changing distance between the probe and the sample during the FE measurements; 2) at more commonly used lower working current the stability should be considerably improved, which has been proposed in previous paper.[30]

For the consideration of device applications, we further investigated the FE characteristics of these two types of thin films on silicon substrates. Fig. 6A compares their $J$–$E$ and FN plots. The turn-on fields (defined as the electric field for $J = 10$ μA cm$^{-2}$) of Sample-Type I and Sample-Type II are 5.0 V μm$^{-1}$ and 4.8 V μm$^{-1}$, respectively, while the threshold fields (defined as the electric field for $J = 1$ mA cm$^{-2}$) are found to be 12.5 and 12.2 V μm$^{-1}$, respectively. The FE properties of Sample-Type II are slightly better than those of Sample-Type I. When the electric field is over 13 V μm$^{-1}$, the emission current density of Sample-Type II is seen to have a much faster increase tendency than Sample-Type I. At 20.7 V μm$^{-1}$, the field emission current density of Sample-Type II arrives at 16.51 mA cm$^{-2}$ while the corresponding value of Sample-Type I is only 9.25 mA cm$^{-2}$, as provided in Table 2. The inset is their corresponding FN plots. The FN plot of Sample-Type II is nearly linear and the FN plot of Sample-Type I may be divided into two straight lines. According to the FN theory, the FN equation is most suitable for metal and may be used to only approximately estimate the emission properties of semiconductors.[58] So the difference in the FN plots suggests that Sample-Type II has metallic properties. From the above comparisons, one may see that Sample-Type II has better field emission properties than Sample-Type I. The possible physical explanation is that some BNTs existing in Sample-Type II can improve its field emission properties due to their higher conductivity. Although the turn-on and threshold field of the sample are still higher than those of the CNTs,[62,63] the existence of the BNTs has improved the FE behaviors in comparison with pure boron nanowires. Once pure BNT films are prepared successfully, they will be more suitable than CNTs in FE applications from the viewpoint of emission uniformity because the conductivity of the boron nanotubes has been proved to be chirality-independent in our above-mentioned measurements.

We further demonstrated their application in one device, *i.e.* the luminescent tube. We first succeeded in growth of the two types of boron nanostructure film on 2 mm diameter stainless

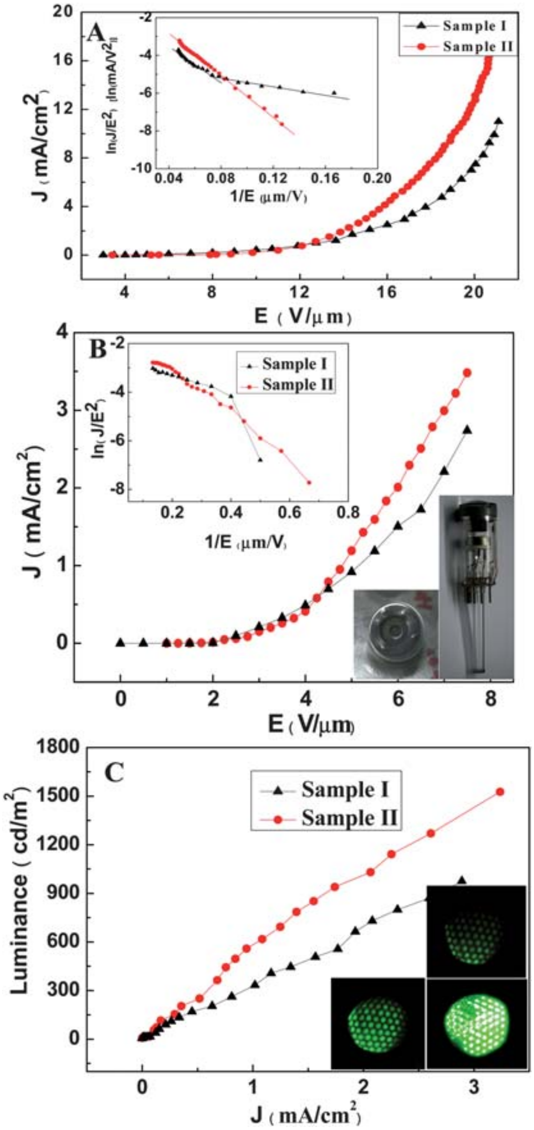

**Fig. 6** (A) The current density *versus* electric field (*J*–*E*) curves of sample I and sample II. The inset is the FN plots of the two samples. (B) The characteristic curves of field emission current *versus* the electric field applied to the extracting gate in a luminescent tube. Left-hand inset corresponds to their FN plots. Right-hand insets show digital camera photos of the nanostructured cathode in a stainless steel substrate and the luminescent tube from our lab. (C) The luminance as a function of extracting gate field. Their operation images at different luminance values (115.4, 443.7 and 1527 cd m$^{-2}$) recorded by CCD are provided in the inset.

steel disk-shape substrates. The electron gun of the luminescent tube was designed by our lab, and the details are described elsewhere.[64,65] During the whole measurement, the voltage applied to the phosphor screen was kept at 5 kV and the pressure in the vacuum chamber was lower than $4 \times 10^{-5}$ Pa. Fig. 6B shows the plots of the total cathode current *versus* the electric field applied to the extracting gate (*I*–*E*) of two luminescent tubes. The right hand inset in Fig. 6B gives the digital photographs of the cathode and the corresponding luminance tube with boron nanostructures. Tube I used a film mixed of boron nanowires and nanotubes and Tube II used only boron nanowires. Tube II has a lower turn-on field (about 2.0 V μm$^{-1}$) and a lower threshold field (about 4.8 V μm$^{-1}$) (at 1 mA cm$^{-2}$) than Tube I. The left-hand inset of Fig. 6B again shows that the FN plot of Tube II is nearly linear while that of Tube I is not. Moreover, as may be seen from Fig. 6C, their luminance increases nearly linearly with the cathode current, which suggests the feasibility in brightness control. At an emission current density of 3 mA cm$^{-2}$, the luminance of Tube II (1412 cd m$^{-2}$) is higher than that of Tube I (1026 cd m$^{-2}$). The inset in Fig. 6C shows the pictures of the luminescent tube at different luminance values in the process of operating, respectively corresponding to cathode current densities of 0.17, 0.76 and 3.23 mA cm$^{-2}$. These two luminescent tubes also exhibit stable luminance operations (initial luminance is set as 637 cd m$^{-2}$), whose fluctuation is less than 7% in 2 h measurements. The two luminescent tubes exhibit stable luminance operations (initial luminance is set as 637 cd m$^{-2}$) with a fluctuation less than 7% in 2 h measurements. Finally, we estimate the DC power consumption for these two luminescent tubes working at threshold field. Based on our designed device structures, about ⅓ of the cathode current $I_{\text{Cathode}}$ is adsorbed by the gate and the other remaining ⅔ of the current can reach the phosphor screen, so the total power consumption $P_{\text{Total}}$ can be calculated by the following expression:

$$P_{\text{Total}} = P_{\text{Gate}} + P_{\text{Anode}} = \frac{1}{3} I_{\text{Cathode}} V_{\text{Gate}} + \frac{2}{3} I_{\text{Cathode}} V_{\text{Anode}} \qquad (3)$$

where $P_{\text{Gate}}$, $P_{\text{Anode}}$, $V_{\text{Gate}}$ and $V_{\text{Anode}}$ are respectively the power of the gate, the power of the anode, the voltage of the gate and the voltage of the anode. The total power consumption is about 79.85 mW for Tube II and 80.92 mW for Tube I, and the power consumption $P_{\text{Gate}}$ is nearly 12 mW for both of them. It is also found that the power efficiency and luminescent efficiency of the two luminescent tubes are respectively over 85% and 0.1 lm W$^{-1}$, which can meet the requirements for lighting devices. Their consumption is still higher than carbon nanotube devices ($P_{\text{Gate}} = 10.72$ mW and $P_{\text{Total}} = 77.7$ mW) reported in ref. 66, which is enough for general commercial displays because it is dramatically lower than many lighting elements, such as light-emitting diodes and cathode-ray tubes using hot filaments. Their performance comparison in luminescent tube applications suggest that the existence of the BNTs maybe beneficial to the tube performance. In addition, the boron nanostructure cold cathode luminescent tube has threshold field performance similar

**Table 2** Comparison of field emission behaviors of Sample-Type I (pure BNW film) and Sample-Type II (film of mixture of BNWs and BNTs)

| Sample type | Average diameter/nm | Average length/μm | Aspect ratio | Electron affinity/eV | β (high field) | Turn on field at 10 μA cm$^{-2}$/V μm$^{-1}$ | Threshold field at 1 mA cm$^{-2}$/V μm$^{-1}$ |
|---|---|---|---|---|---|---|---|
| I | 30 | 5.1 | 170 | 3.74 | 1481 | 5.0 | 12.75 |
| II | 30 | 3 | 100 | 3.24 | 1190 | 4.8 | 12.2 |

to that of a carbon nanotube luminescent tube,[64–66] further indicating that it may be suitable for future outdoor display applications if its operation luminance can be effectively increased to close to carbon nanotubes.

## Conclusions

In summary, we show that BNTs can be synthesized by a thermal evaporation method. The detailed experimental study of crystalline structures of BNTs is reported for the first time. The BNTs are perfect single crystals with a tetragonal structure and their growth direction is along [001]. Measurements on individual BNTs show that their conductivity is in the order of $10^2\ \Omega^{-1}\text{cm}^{-1}$, which is consistent with the theoretical prediction that all the BNTs possess metallic transport properties. Their average 1 nA field and 1 μA field are respectively 50 V $\mu\text{m}^{-1}$ and 55 V $\mu\text{m}^{-1}$, which are much lower than those of BNWs. In addition, individual BNTs can sustain very high current and current density ($\sim$80 μA and $2.04 \times 10^{11}$ A $\text{m}^{-2}$, respectively), which are very close to those reported for carbon nanotubes. Application of films of mixture of BNTs and BNWs and of pure BNWs in luminescent tubes is demonstrated, and it is found that the brightness and the efficiency of the tube using the film consisting of both BNTs and BNWs are better than those using pure BNW film, and that they can be comparable to those with carbon nanotubes.

## Acknowledgements

This work is supported by the National Basic Research Program of China (973 Program, Grant No. 2007CB935500, 863 Program, Grant No. 2007AA03Z305, Science foundation for young scholars, Grant No. 50802117), the National Joint Science Fund with Guangdong Province (Grant No. U0634002, U0734003), the Doctoral Foundation of Education Ministry of China (Grant No. 20070558063 and Grant No. 091gpy28), the Science and Technology Department of Guangdong Province, the Education Department of Guangdong Province, and the Science and Technology Department of Guangzhou City.

## References

1 S. Iijima, *Nature*, 1991, **354**, 56.
2 R. Tenne and A. K. Zetti, *Top. Appl. Phys.*, 2001, **80**, 81.
3 R. Tenne, *Prog. Inorg. Chem.*, 2001, **50**, 269.
4 G. R. Patzke, F. Krumeich and R. Nesper, *Angew. Chem., Int. Ed.*, 2002, **41**, 2446.
5 C. R. Martin, *Science*, 1994, **266**, 1961.
6 P. M. Ajayan, O. Stephan, Ph. Redlich and C. Colliex, *Nature*, 1995, **375**, 564.
7 S. M. Yang, I. Sokolov, N. Coombs, C. T. Kresge and G. A. Ozin, *Adv. Mater.*, 1999, **11**, 1427.
8 U. Kondo and K. Takanayagi, *Science*, 2000, **289**, 606.
9 Y. Li, *J. Am. Chem. Soc.*, 2001, **123**, 9904.
10 Y. Wu and P. Yang, *Adv. Mater.*, 2001, **13**, 520.
11 J. W. G. Wildoer, L. C. Venema, R. E. Smalley and C. Dekker, *Nature*, 1998, **391**, 59.
12 T. W. Odom, J.-L. Huang, P. Kim and C. M. Lieber, *Nature*, 1998, **391**, 62.
13 *Boron and Refractory Borides* (Ed: V. I. Matkovich), Springer, New York, 1977.
14 C. T. Black, K. W. Guarini, K. R. Milkove, S. M. Baker, T. P. Russell and M. T. Tuominen, *Appl. Phys. Lett.*, 2001, **79**, 409.
15 J. Y. Cheng, C. A. Ross, V. Z.-H. Chan, E. L. Thomas, R. G. H. Lammertink and G. J. Vancso, *Adv. Mater.*, 2001, **13**, 1174.
16 T. Thurn-Albrecht, J. Schotter, G. A. Kästle, N. Emley, T. Shibauchi, L. Krusin-Elbaum, K. Guarini, C. T. Black, M. T. Tuominen and T. P. Russell, *Science*, 2000, **290**, 2126.
17 R. R. Li, P. D. Dapkus, M. E. Thompson, W. G. Jeong, C. Harrison, P. M. Chaikin, R. A. Register and D. H. Adamson, *Appl. Phys. Lett.*, 2000, **76**, 1689.
18 I. Boustani, A. Quandt, E. Hernandez and A. Rubio, *J. Chem. Phys.*, 1999, **110**, 3176.
19 A. Gindulyte, W. N. Lipscomb and L. Massa, *Inorg. Chem.*, 1998, **37**, 6544.
20 I. Boustani, *Phys. Rev. B: Condens. Matter*, 1997, **55**, 16426.
21 J. Niu, B. K. Rao and P. Jena, *J. Chem. Phys.*, 1997, **107**, 132.
22 Yiying Wu, Benjanim Messer and Peidong Yang, *Adv. Mater.*, 2001, **13**, 1487.
23 L. M. Cao, Z. Zhang, L. L. Sun, C. X. Gao, M. He, Y. Q. Wang, Y. C. Li, X. Y. Zhang, G. Li, J. Zhang and W. K. Wang, *Adv. Mater.*, 2001, **13**, 1701.
24 L. M. Cao, K. Hahn, Y. Q. Wang, C. Scheu, Z. Zhang, C. X. Gao, Y. C. Li, X. Y. Zhang, L. L. Sun, W. K. Wang and M. Rühle, *Adv. Mater.*, 2002, **14**, 1294.
25 Y. Zhang, H. Ago, M. Yumura, T. Komatsu, S. Ohshima, K. Uchida and S. Iijima, *Chem. Commun.*, 2002, 2806.
26 C. J Otten, O. R. Lourie, M. F. Yu, J. M. Cowley, M. J. Dyer, R. S. Ruoff and W. E. Buhro, *J. Am. Chem. Soc.*, 2002, **124**, 4564.
27 X. M. Meng, J. Q. Hu, Y. Jiang, C. S. Lee and S. T. Lee, *Chem. Phys. Lett.*, 2003, **370**, 825.
28 Q. Yang, J. Sha, J. Xu, Y. J. Ji, X. Y. Ma, J. J. Niu, H. Q. Hua and D. R. Yang, *Chem. Phys. Lett.*, 2003, **379**, 87.
29 D. Ciuparu, R. F. Klie, Y. Zhu and L. Pfefferle, *J. Phys. Chem. B*, 2004, **108**, 3967.
30 F. Liu, J. F. Tian, L. H. Bao, T. Z. Yang, C. M. Shen, X. Y. Lai, Z. M. Xiao, W. G. Xie, S. Z. Deng, J. Chen, J. C. She, N. S. Xu and H. J. Gao, *Adv. Mater.*, 2008, **20**, 2609.
31 X. J. Wang, J. F. Tian, T. Z. Yang, L. H. Bao, C. Hui, F. Liu, C. M. Shen, C. Z. Gu, N. S. Xu and H. J. Gao, *Adv. Mater.*, 2007, **19**, 4480.
32 F. Liu, P. J. Cao, H. R. Zhang, C. M. Shen, Z. Wang, J. Q. Li and H. J. Gao, *J. Cryst. Growth*, 2005, **274**, 126.
33 P. J. Cao, Y. S. Gu, H. W. Liu, F. Shen, Y. G. Wang, Q. F. Zhang, J. L. Wu and H. J. Gao, *J. Mater. Res.*, 2003, **18**, 1686.
34 H. T. Yang, C. M. Shen, Y. K. Su, T. Z. Yang, H. J. Gao and Y. G. Wang, *Appl. Phys. Lett.*, 2003, **82**, 4729.
35 S. T. He, J. N. Yao, P. Jiang, D. X. Shi, H. X. Zhang, S. S. Xie, S. J. Pang and H. J. Gao, *Langmuir*, 2001, **17**, 1571.
36 Terry T. Xu, Alan W. Nicholls and Rodney S. Ruoff, *NANO: Brief Reports and Reviews*, 2006, **1**, 55.
37 Q. Yang, J. Sha, L. Wang, Z. Z. Yuan and D. R. Yang, *Eur. Phys. J. B*, 2007, **56**, 35.
38 Y. Lu, Z. P. Zhu, D. S. Su, D. Wang, Z. Y Liu and R. Schlögl, *Carbon*, 2004, **42**, 3199.
39 W. Richter and K. Ploog, *Phys. Status Solidi B*, 1975, **68**, 201.
40 P. Hohenberg and W. Kohn, *Phys. Rev.*, 1964, **136**, B864.
41 W. Kohn and L. J. Sham, *Phys. Rev.*, 1965, **140**, A1133.
42 W. Guo, Y. B. Hu, Y. Y. Zhang, S. X. Du and H. J. Gao, *Chin. Phys. B*, 2009, **18**, 2502.
43 L. N. Dinh, W. McLean, M. A. Schildbach and M. R. Balooch, *Phys. Rev. B: Condens. Matter Mater. Phys.*, 1999, **59**, 15513.
44 J. van der Weide and R. J. Nemnich, *Phys. Rev. B: Condens.Matter*, 1994, **49**, 13629.
45 M. C. Benjamin, M. D. Bremser, T. W. Weeks, Jr., S. W. King, R. F. Davis and R. J. Nemanich., *Appl. Surf. Sci.*, 1996, **104–105**, 455.
46 *Landolt-Bornstein Numerical Data and Functional Relationships in Science and Technology, New Series* (Ed: K. H. Hellwege), Springer, Berlin, 1983.
47 Ch. Sommerhalter, Th. W. Matthers, Th. Glatzel, A. Jäger-Waldau and M. Ch. Lux-Steiner, *Appl. Phys. Lett.*, 1999, **75**, 286.
48 J. M. R. Weaver and D. W. Abraham, *J. Vac. Sci. Technol., B*, 1991, **9**, 1559.
49 J. C. She, S. An, S. Z. Deng, J. Chen, Z. M. Xiao, J. Zhou and N. S. Xu, *Appl. Phys. Lett.*, 2007, **90**, 073103.
50 T. W. Ebbesen, H. J. Lezec, H. Hiura, J. W. Bennett, H. F. Ghaemi and T. Thio, *Nature*, 1996, **382**, 54.
51 H. J. Dai, E. W. Wong and C. M. Lieber, *Science*, 1996, **272**, 523.

52 B. Q. Wei, R. Spolenak, P. K. Redlich, M. Rühle and E. Arzt, *Appl. Phys. Lett.*, 1999, **74**, 3149.
53 R. H. Fowler and L. W. Nordheim, *Proc. R. Soc. London, Ser. A*, 1928, **119**, 173.
54 Y. Toda, S. W. Kim, K. Hayashi, M. Hirano, T. Kamiya, H. Hosono, T. Haraguchi and H. Yasuda, *Appl. Phys. Lett.*, 2005, **87**, 254103.
55 X. H. Liang, S. Z. Deng, N. S. Xu, J. Chen, N. Y. Huang and J. C. She, *Appl. Phys. Lett.*, 2006, **88**, 111501.
56 J. C. She, N. S. Xu, S. Z. Deng, J. Chen, H. Bishop, S. E. Huq, L. Wang, D. Y. Zhong and E. G. Wang, *Appl. Phys. Lett.*, 2003, **83**, 2671.
57 S. Frank, P. Poncharal, Z. L. Wang and W. A. Deer, *Science*, 1998, **280**, 1744.
58 N. S. Xu and R. V. Latham, *Electron emission based break down mechanisms: Basic Concepts and Technological Practice* (Ed: R. V. Latham), Academic Press: London, 1995, p. 176.
59 J. C. She, Z. M. Xiao, Y. H. Yang, S. Z. Deng, J. Chen, G. W. Yang and N. S. Xu, *ACS Nano*, 2008, **2**, 2015.
60 W. I. Milne, K. B. K. Teo, M. Chhowalla, G. A. J. Amaratunga, S. B. Lee, D. G. Hasko, H. Ahmed, O. Groening, P. Legagneux, L. Gangloff, J. P. Schnell, G. Pirio, D. Pribat, M. Catignolles, A. Loiseau, V. Semet and V. T. Binh, *Diamond Relat. Mater.*, 2003, **12**, 422.
61 Z. Xu, X. D. Bai, E. G. Wang and Z. L. Wang, *Appl. Phys. Lett.*, 2005, **87**, 163106.
62 G. Chen, D. H. Shin, T. Iwasaki, H. Kawarada and C. J. Lee, *Nanotechnology*, 2008, **19**, 415703.
63 R. T. Lv, F. Y. Kang, D. Zhu, Y. Q. Zhu, X. C. Gui, J. Q. Wei, J. L. Gu, D. J. Li, K. L. Wang and D. H. Wu, *Carbon*, 2009, **47**, 2709.
64 J. Chen, X. Zhou, S. Z. Deng and N. S. Xu, *Ultramicroscopy*, 2003, **95**, 153.
65 J. Chen, S. Z. Deng and N. S. Xu, *Ultramicroscopy*, 2003, **95**, 81.
66 Y. Zhang, S. Z. Deng, C. Y. Duan, J. Chen and N. S. Xu, *J. Vac. Sci. Technol., B*, 2008, **26**, 106.